THESIS FOR THE DEGREE OF MASTER OF SCIENCE

Large Eddy Simulation of Channel Flow using Wall Functions

VLADISLAV EFROS

Division of Fluid Dynamics
Department of Applied Mechanics
CHALMERS UNIVERSITY OF TECHNOLOGY

Göteborg, Sweden, 2006

Large Eddy Simulation of Channel Flow using Wall Functions

Vladislav EFROS

Diploma Work

Division of Fluid Dynamics, Department of Applied Mechanics,
Chalmers University of Technology
SE-412 96 Göteborg, Sweden
Phone +46-(0)31-7721400
Fax: +46-(0)31-180976

Printed at Chalmers Reproservice
Göteborg, Sweden 2006

Large Eddy Simulation of Channel Flow using Wall Functions

by
Vladislav EFROS
vladisla@student.chalmers.se
Division of Fluid Dynamics
Department of Applied Mechanics
Chalmers University of Technology
SE-412 96 Göteborg
Sweden

Abstract

Turbulent wall-bounded flows are commonly encountered in engineering practice and are of considerable interests in a variety of industrial applications. This presence of wall significantly affects turbulence characteristics. If we want to solve the near-wall region a very fine mesh is necessary. The number of points needed increases at least like $Re^{1.8}$. This requirement makes LES application of LES for high Reynolds (order of $10^6 - 10^8$) practically impossible.

One solution is to apply near-wall modification, or wall models with a coarse mesh near the wall. When the grid is not fine enough to resolve near-wall structure, the near-wall must be modeled by specifying a correlation between the velocity in first node and shear stress at the wall.

The objective of this study was to implement wall-function for LES simulation of channel flow. The sub-grid scales are modelled using Smagorinsky and Wale model. The first node is placed at $y^+ \sim 49$ for $Re_\tau = 4000$ and $54 \leq y^+ \leq 200$ for $Re_\tau = 16000$. So the first node was located in log-law region and standard wall function was applied. Other modification was introduced in the calculation of the length-scale in the Smagorinsky model using the model proposed by Mason-Callen [7]. Another model introduced was the Werner-Wengler model [6].

Acknowledgement

I would like here to express my gratitude to the persons and institution that made my study possible in Sweden.

My study was financed by the Swedish Institute. I would like to express my sincere gratitude to the Swedish Institute.

I would like to thank:

My supervisor, Professor Lars Davidson, for his great support and encouragement, for his guidance and stimulating discussion during this work.

And, of course, all the people at the Department for their help and support.

Nomenclature

Upper-case Roman

B	Turbulence model constant
C_s	Smagorinsky constant, C_s=0.09
E	Turbulence model constant
H	Non-linear term
G	Filter function
P	Pressure
Re_τ	Reynolds number based on u^*, $u^*\delta/\nu$
S_{ij}	Strain-rate tensor
U	Streamwise mean velocity

Lower-case Roman

f	Damping function
g	Any function
$\overline{g}$	Filtered function
g''	Sub-grid component
l	Length scale
p	Wall adjacent node
t	Time
u_i	Velocity component
U_p	Velocity in first node near the wall
u^*	Friction velocity, $\sqrt{\tau_w/\rho}$
u_{rms}	= $\sqrt{\langle u'^2 \rangle}$
v_{rms}	= $\sqrt{\langle v'^2 \rangle}$
w_{rms}	= $\sqrt{\langle w'^2 \rangle}$
x	Streamwise direction
x_i	Space component
y	Normal direction
z	Spanwise direction

Upper-case Greek

Δt	Time step size
$\Delta x, \Delta y, \Delta z$	Streamwise, normal and spanwise mesh spacings

Lower-case Greek

τ_w	Wall shear stress
δ	Half channel height
κ	Von Karman constant

μ	Dynamic viscosity
ν	Kinematic viscosity
ρ	Density

Abbreviations

CFL	Courant, Friedrichs and Lewy number

subscripts

δ	Quantity based on half channel-width
i	Direction, node number
ij	Tensor indices
n	North face value
p	Node value
w	Wall value

superscripts

n	Time step
u^+	= U_p/u^*
y^+	=$y_p u^*/\nu$

Contents

Chapter 1

LES

1.1 Introduction

Analytical or numerical solution of turbulent flow problems can be accomplished using various levels of approximation, yielding more or less detailed descriptions of the state of flow.

The most used approximation is RANS (Reynolds-averaged Navier-Stokes equations), that has one main draw back: the fact that all scales are modeled in the same way. While the small scales tend to depend only on viscosity, and may be somewhat universal, the large ones are affected very strongly by the boundary conditions. Thus, it doesn't seem possible to model the effect of the large scales of turbulence in the same way in flows that are very different.

The most straightforward approach to the solution of turbulent flow is DNS (Direct Numerical Simulations), but it has some limitations. The main limitation is that one needs to solve all the scales of motion, which requires a number of grid points proportional to the $9/4$ power of the Reynolds number, Re, and the cost of computation scales like Re^3.

The most convenient way between RANS and DNS is to use LES (Large eddy simulations). In LES the contribution of the large scales are computed exactly, and only the effect of the smallest scales is modeled. Since the smallest scales are more homogeneous and universal, and less affected by the boundary conditions than large one, there is hope that their models can be simpler. In LES each quantity g is decomposed as

$$g = \bar{g} + g'' \tag{1.1}$$

where $\bar{g}$ is resolvable-scale component and g'' is small scale or sub-grid (unresolved) component. The $\bar{g}$ is the result of applying a filtering procedure to the local and instantaneous quantities. Filtering is the operation which let us separate the large from the small scales. A filtered variable, denoted by an overbar, is defined as:

$$\bar{g}(x) = \int_D g(x')G(x)(x, x')dx' \tag{1.2}$$

where D is entire domain and G is $filter$ function. The filter function determines the size and structure of small scales. The most common-used filter functions are the sharp Fourier cutoff filter, best defined in wave space:

$$\widehat{G} = \begin{cases} 1\text{: if } k \leq \frac{\pi}{\Delta} \\ 0\text{: otherwise} \end{cases} \tag{1.3}$$

the Gaussian filter,

$$G(x) = \sqrt{\frac{6}{\pi\bar{\Delta}^2}} exp\left(-\frac{6x^2}{\bar{\Delta}^2}\right) \tag{1.4}$$

and the top-hat filter in real space:

$$G(x) = \begin{cases} \frac{1}{\bar{\Delta}} : \text{if } |x| \leq \frac{\bar{\Delta}}{2} \\ 0 \ : \text{otherwise} \end{cases} \tag{1.5}$$

For finite volume method the filtering is the same as the discretisation (integration over the control volume is the same as filtering). The incompressible Navier-Stokes equation before filtering reads:

$$\frac{\partial u_i}{\partial t} + \frac{\partial}{\partial x_j}\left(u_i u_j\right) = -\frac{1}{\rho}\frac{\partial p}{\partial x_i} + \nu\frac{\partial}{\partial x_j}\frac{\partial u_i}{\partial x_j} \tag{1.6}$$

After filtering the Navier-Stokes reads:

$$\frac{\partial \bar{u}_i}{\partial t} + \frac{\partial}{\partial x_j}\left(\bar{u}_i \bar{u}_j\right) = -\frac{1}{\rho}\frac{\partial \bar{p}}{\partial x_i} + \nu\frac{\partial}{\partial x_j}\frac{\partial \bar{u}_i}{\partial x_j} - \frac{\partial \tau_{ij}}{\partial x_i} \tag{1.7}$$

The effect of the small scales is obtained through a subgirdscale (SGS) stress term,

$$\tau_{ij} = \overline{u_i u_j} - \overline{u}_i \overline{u}_j \tag{1.8}$$

that must be modeled. To solve sub-grid component τ_{ij} there are several models, the models used in this work are discussed below.

1.2 Eddy viscosity models

Most sub-grid scale models are eddy-viscosity models of the form,

$$\tau_{ij} - \frac{\delta_{ij}}{3}\tau_{kk} = -2\nu_T \bar{S}_{ij} \tag{1.9}$$

that relate the sub-grid-scale stresses τ_{ij} to the large-scale strain-rate tensor, $\bar{S}_{ij}$.

$$\bar{S}_{ij} = \frac{1}{2}\left(\frac{\partial \bar{u}_i}{\partial x_j} + \frac{\partial \bar{u}_j}{\partial x_i}\right), \tag{1.10}$$

In most cases ν_T is obtained algebraically to avoid solving additional equations that would increase the cost of calculation. Equation (1.9) can be expressed as

$$\tau_{ij} - \frac{1}{3}\delta_{ij}\tau_{kk} = \tau_{ij} - \frac{2}{3}\delta_{ij}\rho\, k' \tag{1.11}$$

where we assumed that $\frac{1}{2}\tau_{kk}/\rho = k'$ Using Eq.(1.11) and Eq.(1.9) into Eq.(1.7), we get

$$\begin{aligned} \frac{\partial \bar{u}_i}{\partial t} + \frac{\partial}{\partial x_j}\left(\bar{u}_i \bar{u}_j\right) &= -\frac{1}{\rho}\frac{\partial \bar{p}_i}{\partial x_i} + \nu\frac{\partial^2 \bar{u}_i}{\partial x_j \partial x_j} \\ &+ \frac{\partial}{\partial x_j}\left\{-\frac{2}{3}\delta_{ij}\rho k' + \nu_T\left[\frac{\partial \bar{u}_i}{\partial x_j} + \frac{\partial \bar{u}_j}{\partial x_i}\right]\right\} \end{aligned} \tag{1.12}$$

Defining pressure as:

$$\bar{P} = \bar{p} + \frac{2}{3}\rho k' \tag{1.13}$$

we obtain:

$$\begin{aligned}\frac{\partial \bar{u}_i}{\partial t} + \frac{\partial}{\partial x_j}\left(\bar{u}_i\bar{u}_j\right) = -\frac{1}{\rho}\frac{\partial \bar{p}_i}{\partial x_i} &+ \nu\frac{\partial^2 \bar{u}_i}{\partial x_j \partial x_j} \\ &+ \frac{\partial}{\partial x_j}\left\{\nu_T\left[\frac{\partial \bar{u}_i}{\partial x_j} + \frac{\partial \bar{u}_j}{\partial x_i}\right]\right\}\end{aligned} \tag{1.14}$$

To solve Eq.(1.14) we need a relation for ν_T. How to obtain ν_T is described below.

1.3 The Smagorinsky model

For the Smagorinsky model the ν_T is obtained:

$$\nu_T = l^2|\bar{S}| \tag{1.15}$$

where the strain-rate tensor $|\bar{S}|$ is calculated as:

$$|\bar{S}| = \left(2\bar{S}_{ij}\bar{S}_{ij}\right)^{1/2} \tag{1.16}$$

$$l = C_s\overline{\Delta} \tag{1.17}$$

$$C_s = 0.09 \tag{1.18}$$

When the grid is inhomogeneous the filter width is given by $\bar{\Delta} = (\Delta x \Delta y \Delta z)^{\frac{1}{3}}$. Furthermore in the presence of solid boundaries the length scale needs to be modified by the introduction of van Driest damping function to account for the reduced growth of the small scales near the wall; hence the model will look like:

$$\nu_T = \left(C_s\bar{\Delta}f\right)^2|\bar{S}| \tag{1.19}$$

where f is damping function:

$$f = 1 - e^{-y^+/25} \tag{1.20}$$

1.4 The Wale Model

The Smagorinsky model by construction gives a non zero value for ν_T as soon as there is a velocity gradient. Near the wall however the turbulent fluctuations are damped so that $\nu_T \to 0$. One way to produce zero eddy viscosity is to make C_s to go to zero as was proposed by Germano with his dynamical model. However this procedure often leads to a negative value of C_s and thus may generate numerical instability. In LES, the eddy-viscosity ν_T must not change when the frame of reference is changed. Clearly the velocity gradient tensor $\bar{g}_{ij} = \partial\bar{u}_i/\partial x_j$ is a good choice to represent velocity fluctuations at the length scale Δ. The Smagorinsky model is based on the second invariant of the symmetric part $\bar{S}_{ij}$ of this tensor. There are two major drawback associated with this choice:

- this invariant is only related to the strain rate of the turbulent structure but not the rotation rate,
- this invariant is of order $\mathcal{O}(1)$ near wall

A better way to build a better operator is to consider the traceless symmetric part of the square of the velocity gradient tensor:

$$S_{ij}^d = \frac{1}{2}\left(\bar{g}_{ij}^2 + \bar{g}_{ji}^2\right) - \frac{1}{3}\delta_{ij}\bar{g}_{kk}^2, \tag{1.21}$$

where $\bar{g}_{ij}^2 = \bar{g}_{ik}\bar{g}_{kj}$ and δ_{ij} is the Kronecker symbol. Let us denote $\bar{\Omega}$ the anti-symmetric part of $\bar{g}$:

$$\bar{\Omega}_{ij} = \frac{1}{2}\left(\frac{\partial \bar{u}_i}{\partial x_j} - \frac{\partial \bar{u}_j}{\partial x_i}\right) \tag{1.22}$$

The tensor S_{ij}^d can be rewritten in terms of $\bar{S}$ and $\bar{\Omega}$. One obtains:

$$S_{ij}^d = \bar{S}_{ik}\bar{S}_{kj} + \bar{\Omega}_{ik}\bar{\Omega}_{kj} - \frac{1}{3}\delta_{ij}\left[\bar{S}_{mn}\bar{S}_{mn} - \bar{\Omega}_{mn}\bar{\Omega}_{mn}\right] \tag{1.23}$$

By construction, the trace of S^d is zero and its second invariant remains finite and proportional to $S_{ij}^d S_{ij}^d$. By using the relation above and making use of the Cayley-Hamilton theorem of linear algebra, this quantity can be developed as (assuming incompressibility):

$$S_{ij}^d S_{ij}^d = \frac{1}{6}\left(S^2S^2 + \Omega^2\Omega^2\right) + \frac{2}{3}S^2\Omega^2 + 2IV_{S\Omega} \tag{1.24}$$

with the notations:

$$S^2 = \bar{S}_{ij}\bar{S}_{ij},\ \Omega^2 = \bar{\Omega}_{ij}\bar{\Omega}_{ij},\ IV_{S\Omega} = \bar{S}_{ik}\bar{S}_{kj}\bar{\Omega}_{jl}\bar{\Omega}_{li}$$

From the last relation, a LES model based on $S_{ij}^d S_{ij}^d$ will detect turbulence structures with either (large) strain rate, rotation strain or both. In the case of pure shear (e.g., $\bar{g}_{ij} = 0, \text{ except } \bar{g}_{12}$, it yields $S^2 = \Omega^2 = 4\bar{S}_{12}$ and $IV_{S\Omega} = -\frac{1}{2}S^2S^2$, so that the considered invariant, $S_{ij}^d S_{ij}^d$, is zero. This point is in agreement with the fact that the shear zones contribute to energy dissipation to a smaller extent than convergence zones and eddies. Moreover, this mean that almost no eddy viscosity would be produced in the case of wall-bounded laminar flow (Poiseuille flow). Thus the amount of turbulence diffusion would be negligible in such a case and the development of linearly unstable waves would be possible. This is a great advantage over the Smagorinsky model which is unable to reproduce the laminar to turbulent transition of such flow due to the invariant $\bar{S}_{ij}\bar{S}_{ij}$ is large in case of pure shear. Using Taylor expansion for velocities can be shown that $-\overline{uv}$ behaves like y^3 while $S_{ij}^d S_{ij}^d$ behaves like y^2. We know that ν_T should behave like y^3 so the expression for ν_T is [8]:

$$\nu_T = (C_S\Delta)^2 \frac{\left(S_{ij}^d S_{ij}^d\right)^{\frac{3}{2}}}{\left(\bar{S}_{ij}\bar{S}_{ij}\right)^{\frac{5}{2}} + \left(S_{ij}^d S_{ij}^d\right)^{\frac{5}{4}}} \tag{1.25}$$

Chapter 2

Wall Functions

2.1 Introduction

At solid walls, the momentum flux must be known. Since the wall velocity is assigned, the no-slip condition allows the determination of the convective part $u_i u_j$ of the momentum flux at the wall. Differentiation of the velocity profile to determine the viscous stress, however is accurate only if the wall layer is well-resolved.

To represent accurately the structures in the near-wall region, the first grid point must be located at $y^+ < 1$, and the grid spacing must be of order $\Delta x^+ \simeq 50 - 150,\ \Delta z^+ \simeq 15 - 40$ for LES[9]. As $Re \rightarrow \infty$, an increasing number of grid points must be used to resolve a layer of decreasing thickness. This may also result in high aspect-ratio cells, with subsequent degradation of the numerical accuracy.

Alternatively, approximate boundary conditions, or wall models may be used in LES. When the grid is not fine enough to resolve the gradients near the wall, there should be specified a law which correlate the outer flow (the velocity in first grid point) and the shear stress at the wall. This allows us to place the first node at $y^+ \approx 30 - 200$.

This idea practically means that the first computational node is placed $outside$ the viscous sublayer, and that suitable assumptions about how the near-wall velocity profile behaves are made, in order to obtain the wall shear stress.

The drawback of this method is that it will not give an accurate approximation of the velocity gradient, and hence the shear stress, at the wall.

The advantage is in improving convergence and reducing the computational time, with accepted deterioration in results.

2.2 Log-law

According to Lumley[5] the boundary layer region can be divided into three different regions:

- viscous sub-layer $0 < y^+ < 5$

  At the surface all the stress is viscous stress. The question is if the Reynolds stress contribute to the stress at small value of y^+? Experimental evidence has shown that the Reynolds stress remains a small fraction of u^{*2} up to about $y^+ = 5$. This layer is called

viscous sublayer. In viscous sublayer, the flow is not steady, but the velocity fluctuations do not contribute much to the total stress because of the viscosity. In the viscous sublayer we should have $u^+ = y^+$.

- buffer layer $5 < y^+ < 30$

  The region where neither one of the stresses can be neglected is called the buffer layer. This is the region where the linear velocity in the viscous layer is linked to logarithmic velocity profile in the inertial sublayer.

- inertial sub-layer $30 < y^+ < 200$

  In the literature, the inertial layer is called the logarithmic region because its mean-velocity profile is logarithmic.

$$U^+ = \frac{1}{\kappa} \ln y^+ + B \tag{2.1}$$

or using the definition for u^+ and y^+ we obtain:

$$U_p = \frac{u^*}{\kappa} \ln \left(\frac{y_p u^*}{\nu} \right) + B \tag{2.2}$$

2.3 Standard wall Functions

The logarithmic law (2.2) is directly applied to first interior node. In a turbulent boundary-layer, the strongest velocity gradient is found near the wall. With a wall function based turbulence model, which utilizes a relatively coarse mesh, it is impossible to resolve these wall

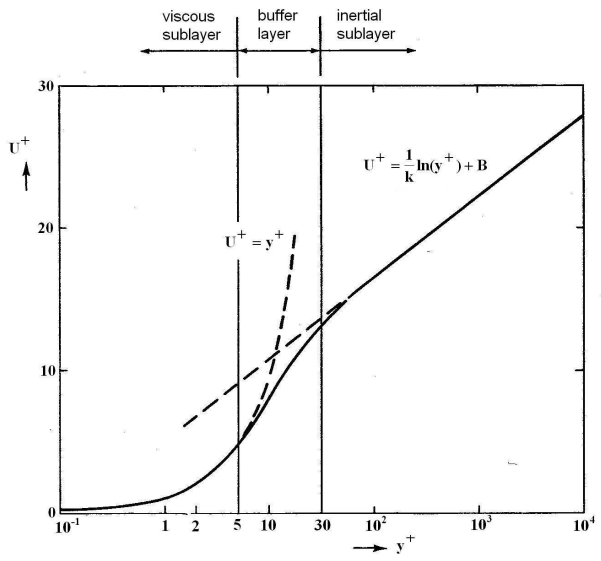

Figure 2.1: The law of the wall

gradient [1]. The predicted wall friction would thus be largely in error if a modification is not introduced:

$$\tau_w = \mu \frac{\partial U}{\partial y} > \mu_e \frac{\delta U}{\delta y} = \mu_e \frac{U_p}{y_p} \tag{2.3}$$

where the subscript p is used for first interior node. The necessary modification could either be made through:

1. an added source term simulating the correct wall friction or
2. a modified viscosity, an effective viscosity, μ_e, that ensures the correct friction even though the velocity gradient is erroneous.

Through the law-of-the-wall:

$$\frac{U}{u^*} = \frac{1}{\kappa} \ln\left(Ey^+\right) \tag{2.4}$$

the wall friction is computed as:

$$\tau_w = \frac{\rho u^* U \kappa}{ln\left(Ey^+\right)} \tag{2.5}$$

with $\tau_w = \rho u^{*2}$.

2.4 The Werner-Wengle model

According to Werner-Wengler[6] the boundary conditions at horizontal walls are specified by assuming that at the grid points (p) closest to the wall, (a) the instantaneous velocity components tangential to the wall (u_p, w_p) are in phase with the instantaneous wall shear stress components (τ_{ub}, τ_{wb}) and (b) the instantaneous velocity distribution is assumed to follow the linear law-of-the-wall,

$$u^+ = y^+ \qquad \text{for} \qquad y^+ \leq 11.81 \tag{2.6}$$

and it is continued by power-law description

$$u^+ = A(y^+)^B \qquad \text{for} \qquad y^+ = y_m > 11.81 \tag{2.7}$$

with A=8.3 and B=1/7. The velocity components tangential to a wall at the grid point next to the wall (u_p, w_p) can be related to the corresponding wall shear stress components by integrating the velocity distribution over the height of the first control volume.

According to definition:

$$\begin{aligned} u^+ &= \frac{U_p}{u^*} \\ y^+ &= \frac{y_p u^*}{\nu} \\ \nu &= \frac{\mu}{\rho} \end{aligned}$$

The intersection of the two laws, linear and power will give us,

$$y^+ = A^{\frac{1}{1-B}} = y_m^+$$

where subscript m denotes the intersection point.

$$\frac{U_p}{u^*} = \frac{y_p u^*}{\nu} \Rightarrow \; u^{*2} = \frac{U_p \nu}{y_p} \tag{2.8}$$

$$\tau_w = \rho u^{*2} = \rho \frac{U_p \mu}{y_p \rho} = \frac{2 U_p \mu}{\Delta y} \tag{2.9}$$

For the $\Delta y^+ \leq y_m^+$ we get:

$$\begin{aligned} u^+ &= \frac{1}{\Delta y^+} \int_0^{\Delta y^+} y^+ \, \mathrm{d}y^+ = \frac{1}{\Delta y^+} \frac{y^{+2}}{2} \Big|_0^{\Delta y^+} \\ &= \frac{1}{2\Delta y^+} A^{\frac{2}{1-B}} \end{aligned} \tag{2.10}$$

In Eq.(2.10) using the definition of u^+ and y^+,

$$U_p = \frac{\mu}{2\rho \Delta y} A^{\frac{2}{1-B}} \tag{2.11}$$

The Eq.(2.11) expresses the maximum velocity for linear-law.

So for $\Delta y^+ \leq y_m^+$ we have

$$|\tau_{ub}| = \frac{2\mu |U_p|}{\Delta y} \tag{2.12}$$

for

$$|U_p| \leq \frac{\mu}{2\rho \Delta y} A^{\frac{2}{1-B}} \tag{2.13}$$

If for our next node to the wall we have $\Delta y^+ > y_m^+$ we should use the power law description for velocity Eqn.(2.7). We have to integrate velocity along the height (Δy) of the first cell near the wall.

$$\begin{aligned} u^+ &= \frac{1}{\Delta y^+} \int_0^{\Delta y^+} u^+(y^+) \, \mathrm{d}y^+ \\ &= \frac{1}{\Delta y^+} \left(\int_0^{y_m^+} u_1^+(y^+) \, \mathrm{d}y^+ + \int_{y_m^+}^{\Delta y^+} u_2^+(y^+) \, \mathrm{d}y^+ \right) \end{aligned} \tag{2.14}$$

where for $u_1^+(y^+)$ we will use linear-law Eqn.(2.6) and for $u_2^+(y^+)$ power-law profile Eqn.(2.7) see Fig.2.2. Using enq.(2.6) and Eqn.(2.7) in enq.(2.14) we obtain:

$$\begin{aligned} u^+ \Delta y^+ &= \int_0^{y_m^+} y^+ \, \mathrm{d}y^+ + \int_{y_m^+}^{\Delta y^+} A \left(y^+\right)^B \, \mathrm{d}y^+ \\ &= \frac{y^{+2}}{2} \Big|_0^{y_m^+} + \frac{A}{1+B} \left(y^+\right)^{(1+B)} \Big|_{y_m^+}^{\Delta y^+} \\ &= \frac{y_m^{+2}}{2} + \frac{A}{1+B} \left(\left(\Delta y^+\right)^{1+B} - \left(y_m^+\right)^{1+B} \right) \end{aligned}$$

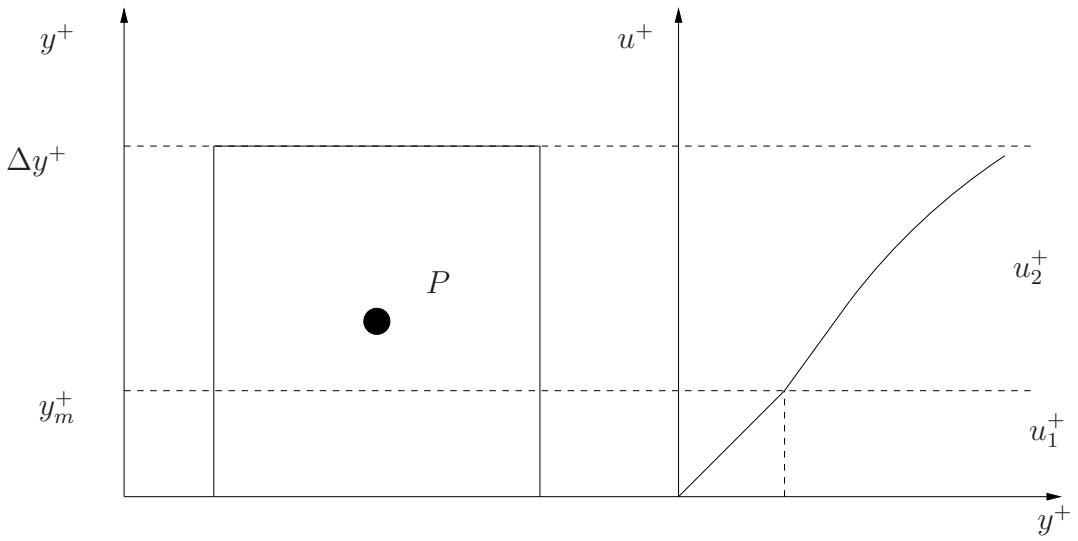

Figure 2.2: The Werner-Wengler model

$$\begin{aligned}
\frac{U_p}{u^*}\frac{\Delta y u^*}{\nu} &= \frac{1}{2}A^{\frac{2}{1-B}} + \left(\frac{\Delta y u^*}{\nu}\right)^{1+B}\frac{A}{1+B} - \frac{A}{1+B}A^{\frac{1+B}{1-B}} \\
U_p\frac{1+B}{A}\frac{\Delta y}{\nu} &= \frac{1}{2}A^{\frac{2}{1-B}}\frac{1+B}{A} + \left(\frac{\Delta y}{\nu}\right)^{1+B} u^{*(1+B)} - A^{\frac{1+B}{1-B}}
\end{aligned} \tag{2.15}$$

From Eqn.(2.15) we can write an expression for u^*

$$\begin{aligned}
u^{*(1+B)} &= \frac{1+B}{A}\left(\frac{\nu}{\Delta y}\right)^B U_p - \frac{1+B}{2}A^{\frac{1+B}{1-B}}\left(\frac{\nu}{\Delta u}\right)^{1+B} + A^{\frac{1+B}{1-B}}\left(\frac{\nu}{\Delta u}\right)^{1+B} \\
&= \frac{1+B}{A}\left(\frac{\nu}{\Delta y}\right)^B U_p + \frac{1-B}{2}\left(\frac{\nu}{\Delta y}\right)^{1+B} A^{\frac{1+B}{1-B}}
\end{aligned} \tag{2.16}$$

with $\tau_w = \rho u^{*2}$ we obtain,

$$\tau_w = \rho\left[\frac{1+B}{A}\left(\frac{\nu}{\Delta y}\right)^B U_p + A^{\frac{1+B}{1-B}}\left(\frac{\nu}{\Delta y}\right)^{1+B}\left(\frac{1-B}{2}\right)\right]^{\frac{2}{1+B}} \tag{2.17}$$

Hence,

$$|\tau_w| = \rho\left[\frac{1-B}{2}A^{\frac{1+B}{1-B}}\left(\frac{\mu}{\rho\Delta y}\right)^{1+B} + \frac{1+B}{A}\left(\frac{\mu}{\rho\Delta y}\right)^B |U_p|\right]^{\frac{2}{1+B}} \tag{2.18}$$

$$\text{for} \quad |U_p| > \frac{\mu}{2\rho\Delta y}A^{\frac{2}{1-B}} \tag{2.19}$$

2.5 The Mason-Callen model

To simulate a channel flow a second-order numerical scheme is used. The sub-grid parametrization is of form proposed by Mason-Callen [7].

2.5.1 Sub-grid parametrization

This model is the local equilibrium limit of transport equation to determine the sub-grid-scale energy, i.e.

$$\tau_{ij} = \nu \left(\frac{\partial \bar{u}_i}{\partial x_j} + \frac{\partial \bar{u}_j}{\partial x_i} \right) \tag{2.20}$$

$$\nu_T = l^2(y)|\overline{S}|, \tag{2.21}$$

where $l(y)$ is a prescribed function varying with y. The computational mesh used to resolve the y-direction has a fairly uniform value in the interior of the channel but is refined near walls. Since there is no corresponding refinement in the span-wise and stream-wise meshes there is little scope for resolving small eddies near the walls: $l(y)$ is thus not linked to mesh variations. A fixed basic value l_0 is specified and near the walls small three-dimensional eddies are represented by a Prandtl mixing-length. This in turn allows a match to the law of the wall, i.e. we require

$$l(y) \sim \kappa\,(y + y_0) \;\; as \; y \to 0 \tag{2.22}$$

To link this near-wall Prandtl mixing length to the interior value we take

$$\frac{1}{l} = \frac{1}{l_0} + \frac{1}{\kappa\,(y + y_0)} + \frac{1}{\kappa\,(2\delta - y + y_0)} \tag{2.23}$$

where κ is Von Karmans constant and $y = 0$ and $y = 2\delta$ are the boundaries of the channel with midpoint $y = \delta$, y_0 is the surface roughness length for a high-Reynolds number flow. The relation between l_0 and C_s defined as,

$$C_s = \frac{l_0}{(\Delta x \Delta y_{max} \Delta z)^{\frac{1}{3}}} \tag{2.24}$$

where Δx and Δz are the constant grid intervals in the stream-wise and span-wise directions respectively and Δy_{max} represent the maximum (in practice a typical value) grid interval across the channel.

Chapter 3

Test Case

The case chosen for simulation in this work is a flow in a channel. The geometry of the computational domain is given in Fig (3.2). The Reynolds number Re_{tau} based on the half height of channel δ is 4000 and 16000.

3.1 The balance of mean forces

We consider a fully developed channel flow. We assume that nothing changes in z direction and that $\langle W \rangle$ is zero. We also assume that $\langle U \rangle$ is not a function of x, since the profile is fully developed. With this assumptions the continuity equation reduces to,

$$\frac{d\langle V \rangle}{dy} = 0 \tag{3.1}$$

With the boundary conditions $\langle V \rangle_{y=0}$, this dictates that $\langle V \rangle$ is zero for all y, so that the boundary condition at the top wall$\langle V \rangle_{y=2\delta}$ is also satisfied. From y-direction momentum, we have,

$$0 = -\frac{d}{dy}\langle v^2 \rangle - \frac{1}{\rho}\frac{\partial \langle P \rangle}{\partial y} \tag{3.2}$$

which, with the boundary condition $\langle v^2 \rangle_{y=0} = 0$ and $\langle v^2 \rangle_{y=\delta} \neq 0$, integrates to,

$$\langle v^2 \rangle + \langle P \rangle / \rho = P_w(x)/\rho \tag{3.3}$$

where P_w is the mean pressure on the bottom of the wall. An important result from this equation is that the mean axial pressure gradient is uniform across the flow:

$$\frac{\partial \langle P \rangle}{\partial x} = \frac{dP_w}{dx} \tag{3.4}$$

The momentum equation in x-direction,

$$0 = \nu \frac{d^2\langle U \rangle}{dy^2} - \frac{d}{dy}\langle uv \rangle - \frac{1}{\rho}\frac{\partial \langle P \rangle}{\partial x} \tag{3.5}$$

can be rewritten,

$$\frac{d\tau}{dy} = \frac{dP_w}{dx} \tag{3.6}$$

where the total shear stress $\tau(y)$ is

$$\tau = \rho\nu\frac{d\langle U\rangle}{dy} - \rho\langle uv\rangle \tag{3.7}$$

For this flow there is no acceleration, so the mean momentum equation Eqn.(3.6) amounts to a balance of forces: the axial pressure gradient is balanced by the shear-stress term.

Since τ is a function of y, and P_w is a function only of x it is evident from Eqn.(3.6) that both $d\tau/dy$ and dP_w/dx are constant. The solution for $\tau(y)$ and dP_w/dx can be written explicitly in terms of the $wall\ shear\ stress$.

Because $\tau(y)$ is antisymmetric about mid-plane, it follows that $\tau(\delta)$ is zero; and at the top wall the stress $\tau(2\delta) = -\tau_w$ see Fig.3.1.

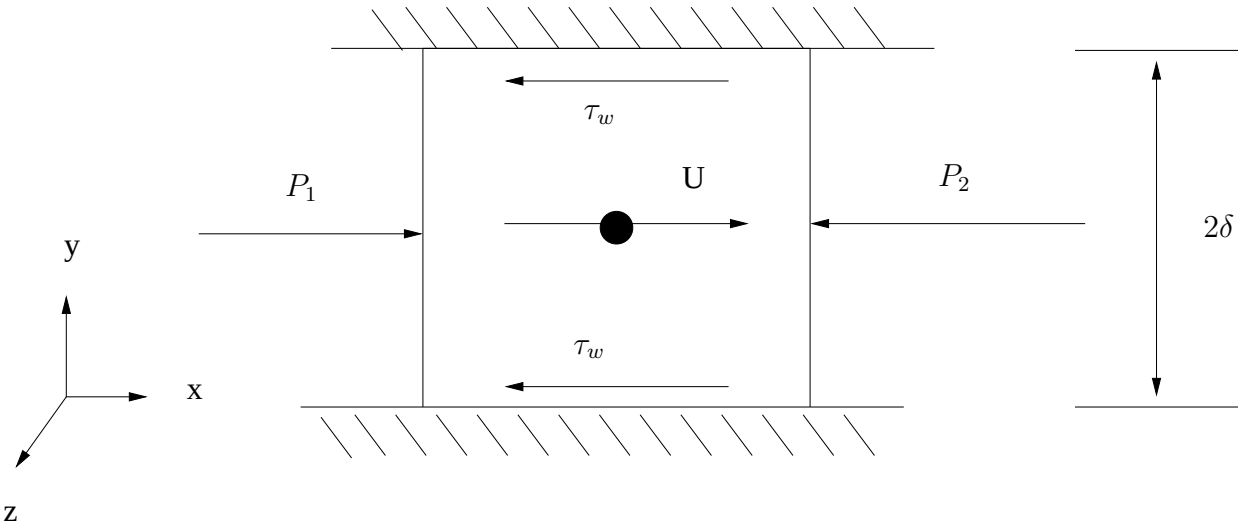

Figure 3.1: The balance of mean forces

Hence, the integration of Eqn.(3.6) from 0 to 2δ yields,

$$-\frac{dP_w}{dx} = \frac{\tau_w}{\delta} = -\frac{\partial\langle P\rangle}{\partial x} \tag{3.8}$$

and

$$\tau(y) = \tau_w\left(1 - \frac{y}{\delta}\right) \tag{3.9}$$

$$\frac{dP}{dx} = \frac{d\tau}{dy} \tag{3.10}$$

after integration from 0 to 2δ

$$\frac{\tau_w}{\delta} = -\frac{dP}{dx} \equiv 1 \tag{3.11}$$

The term $dP/dx \equiv 1$ is added in source term.

3.2 Boundary conditions

The following boundary conditions were applied:

- In y direction we have no-slip conditions at $y = 0$ and $y = 2\delta$
- in x and z directions we have periodic boundary conditions.

Periodic boundary conditions implies that the computational domain repeats itself an infinite number of times. Periodic boundary conditions are convenient, since they eliminate the need to specify inflow and outflow conditions. They are easy to implement and efficient, since they allow use of small computational domain. The use of periodic boundary conditions is similar to studying time development, rather than the spatial development, of a flow.

Mesh	Nodes	Δx	Δz	Stretching ratio	Re_δ	y_p^+
A	34x34x34	0.094	0.0467	1.115	4000	49
B	34x60x34	0.094	0.0467	1.100	16000	54
C	34x60x34	0.094	0.0467	1.060	1600	108
D	34x60x34	0.094	0.0467	1.022	1600	200
E	34x34x60	0.094	0.0129	1.115	4000	49
F	50x34x60	0.031	0.0129	1.115	4000	49
G	50x82x60	0.031	0.0129	1.00122	4000	49
H	34x82x34	0.094	0.0467	1.00122	4000	49

Table 3.1: Geometrical and numerical details of the meshes
Index p denotes the wall adjacent node

3.3 Computational Grid

Several grids were used, and they are given in Table (3.1). A grid stretching was used in the y directions and a uniform grid in the other two directions.

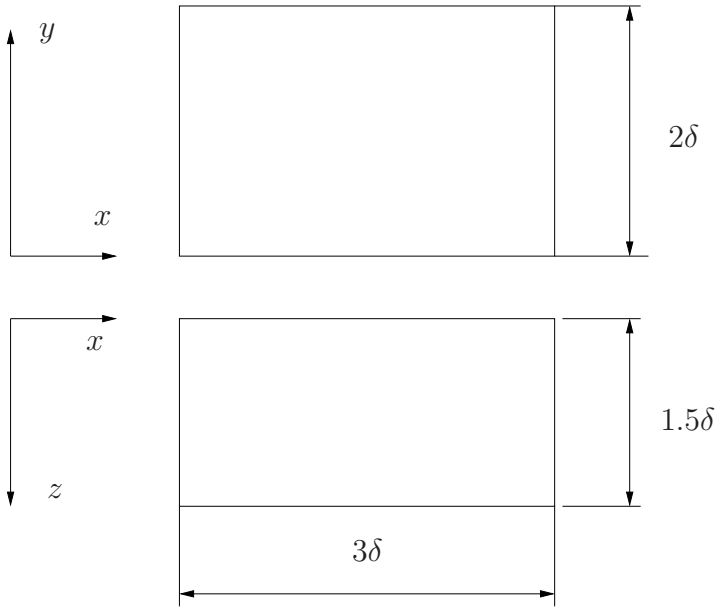

Figure 3.2: Geometry of the test case

Chapter 4

Implementation of Wall Functions

4.1 General description of the code

Calculation are performed using the CALC-BFC code. The code CALC-BFC is based on a 3 - D finite volume method for solving the incompressible Navier-Stokes equations. The code uses collocated variable arrangement in which all variables are stored at the same control volume. The convective fluxes are approximated using central differencing scheme. Because of periodic boundary condition a CTDMA (Cycle-Tri-Diagonal-Matrix Algorithm) is utilized to solve the algebraic relations obtained after discretisation. A Crank-Nicolson scheme is used for time integration [4].

4.2 The Method

The CALC-BFC code uses an implicit two-step time-advancement method [3]. Integration of Eq.(1.14] from t and $t + \Delta t$ gives:

$$\bar{u}_i^{n+1} = \bar{u}_i^n + \Delta\, tH\left(\bar{u}_i^n, \bar{u}_i^{n+1}\right) - \frac{1}{\rho}\alpha\Delta t\frac{\partial p^{n+1}}{\partial x_i} - \frac{1}{\rho}\left(1-\alpha\right)\Delta t\frac{\partial p^n}{\partial x_i} \tag{4.1}$$

The intermediary velocity at time step $n + 1/2$ is,

$$\bar{u}_i^{n+1/2} = \bar{u}_i^n + \Delta\, tH\left(\bar{u}_i^n, \bar{u}_i^{n+1/2}\right) - \frac{1}{\rho}\alpha\Delta t\frac{\partial p^{n+1/2}}{\partial x_i} - \frac{1}{\rho}\left(1-\alpha\right)\Delta t\frac{\partial p^n}{\partial x_i} \tag{4.2}$$

The theory behind this method is the idea that a vector field can be broken in two parts, one part that is of zero curl and a portion that is of zero divergence.

For the moment we have to ignore pressure (no implicit pressure).

$$\bar{u}_i^{n+\frac{1}{2}} = \bar{u}_i^n + \Delta\, tH\left(\bar{u}_i^n, \bar{u}_i^{n+1/2}\right) - \alpha\Delta\, t\frac{\partial \bar{p}^{n+1/2}}{\partial x_i} \tag{4.3}$$

where $H(u_i^n, u^{n+1/2})$ includes the convective term and viscous and SGC stresses; $\alpha = 0.5$ (Crank-Nicholson method). In SIMPLE notation Eqn.(4.3) has the form,

$$a_p\bar{u}_i^{n+1/2} = \sum a_{nb}\bar{u}^{n+1/2} + S_U - \alpha\Delta t\frac{\partial \bar{p}^{n+1/2}}{\partial x_i}\Delta V \tag{4.4}$$

where S_U include all source terms except implicit pressure.

From Eqn.(4.3) we obtain $\bar{u}_i^{n+1/2}$ which doesn't satisfy continuity. An intermediate velocity field is computed,

$$\bar{u}_i^* = \bar{u}_i^{n+1/2} + \frac{1}{\rho}\alpha\Delta t\frac{\partial \bar{p}^{n+1/2}}{\partial x_i} \tag{4.5}$$

The pressure is recovered by defining u^{n+1} as follows:

$$\bar{u}_i^{n+1} = \bar{u}_i^* - \frac{1}{\rho}\alpha\Delta t\frac{\partial p^{n+1}}{\partial x_i} \tag{4.6}$$

By solving (4.5) for u^* and inserting in (4.6), we see that we obtain,

$$\bar{u}_i^{n+1} = \bar{u}_i^n + \Delta\, tH\left(\bar{u}_i^n, \bar{u}_i^{n+1}\right) - \frac{\alpha}{\rho}\Delta t\frac{\partial p^{n+1}}{\partial x_i} - \frac{(1-\alpha)}{\rho}\Delta t\frac{\partial p^n}{\partial x_i} \tag{4.7}$$

Now if we take divergence from Eq.(4.6),

$$\frac{\partial \bar{u}_i^{n+1}}{\partial x_i} = \frac{\partial \bar{u}_i^*}{\partial x_i} + \frac{1}{\rho}\alpha\Delta\frac{\partial^2 p^{n+1}}{\partial x_i \partial x_i} \tag{4.8}$$

Now we require that the face velocities $\bar{u}_{i,f}^{n+1}$(which are obtained by linear interpolation) satisfy the continuity equation $\partial \bar{u}_{i,f}^{n+1}/\partial x_i = 0$, we will end with Poisson equation for the pressure:

$$\frac{\partial^2 p^{n+1}}{\partial x_i \partial x_i} = \frac{\rho}{\Delta t\alpha}\frac{\partial \bar{u}_{i,f}^*}{\partial x_i} \tag{4.9}$$

The numerical procedure at each time step is following:

1. Solve the Navier-Stokes equation for $\bar{u}, \bar{v}, \bar{w}$.
2. Create an intermediate velocity field using Eqn.(4.5)
3. Solve Poisson equation (4.9)
4. Compute the face velocities $\bar{u}_{i,f}^{n+1}$ (which satisfy continuity) from the pressure and the intermediate velocity using

$$\bar{u}_{i,f}^{n+1} = \bar{u}_{i,f}^* - \frac{1}{\rho}\alpha\Delta t\left(\frac{\partial p^{n+1}}{\partial x_i}\right)_f \tag{4.10}$$

5. Compute turbulent viscosity ν_T
6. Step 1 to 5 until convergence is reached.
7. Next time step

4.3 Computation of ν_T

To calculate ν_T the Smagorinsky and the Wale model were used. For the Smagorinsky model the length scale was calculated in two different ways:

- Firstly the length scale was calculated like:

$$\begin{aligned} l_{min} &= min\left(l_{RANS}, l_{LES}\right) \\ \text{where} & \\ l_{RANS} &= k y_p \\ l_{LES} &= C_s \left(\Delta x \Delta y \Delta z\right)^{\frac{1}{3}} \end{aligned} \tag{4.11}$$

- Secondly the Mason-Callen model was implemented

$$\frac{1}{l} = \frac{1}{C_s \left(\Delta x \Delta y \Delta z\right)^{\frac{1}{3}}} + \frac{1}{\kappa \cdot min(y_p, 2 - y_p)} \tag{4.12}$$

In both cases the length scale is a function of (i,j,k). A comparison of length scales used, l_{min} and l_{mason}, is shown in Fig. (4.1). The length scale l_{min} is almost two times larger than l_{mason} in the near wall region, resulting in difference of sub-grid dissipation. Even with the damp function Eqn.(1.20), the classical Smagorinsky model is more dissipative than the Mason-Callen model.

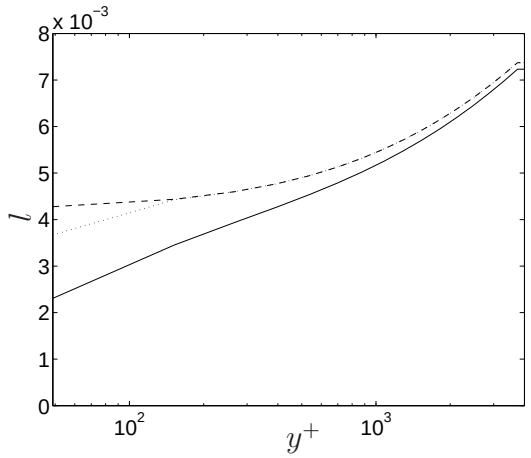

Figure 4.1: Comparison of length scale for Smagorinsky model:$--l_{min}$, $-l_{mason}$, $\cdots l_{min} \cdot f$

4.4 Implementation of wall function

The wall function are implemented via modified viscosity at the wall and via source term for the Werner-Wengler model.

- According to log-law,

$$\begin{aligned} \tau_w &= \mu \frac{\partial U}{\partial x}|_{y^+\approx 1} \\ \tau_w &= \mu_{T,w} \frac{\partial U}{\partial x}|_{y^+>30} \approx \mu_{T,w} \frac{U}{y} \\ \tau_w &= \rho u^{*2} \\ &\text{we obtain} \\ \mu_{T,w} &= \frac{u^*}{U_p} \rho u^* y_p \\ &\text{using } \log - \text{law} \\ \frac{U_p}{u^*} &= \frac{1}{\kappa} \ln\left(E y^+\right) \\ &\text{the result is} \\ \mu_{T,w} &= \frac{\rho u^* y_p \kappa}{\ln E y_p^+} \end{aligned} \tag{4.13, 4.14}$$

- In the discretized momentum equation,

$$a_p U_p = a_e U_e + a_w U_w + a_n U_n + a_s U_s + a_t U_t + a_b U_b + S_u \tag{4.15}$$

a_s arises from the shear stress at the south face of the cell see Fig. (4.2). Because we obtain the wall shear stress from an assumed velocity profile, we can set $a_s = 0$ and then add the wall shear stress $\tau_w \Delta x \Delta z$ directly into the source term.

The general source term S is expressed as:

$$S = S_p \Phi_p + S_u \tag{4.16}$$

where $\Phi = U$ because the Werner-Wengler model was implemented only for U component; the Werner-Wengler equation for τ_w is

$$|\tau_w| = \rho \left(\frac{1+B}{A} \left(\frac{\nu}{\Delta y} \right)^B |U_p| + A^{\frac{1+B}{1-B}} \left(\frac{\nu}{\Delta y} \right)^{1+B} \left(\frac{1-B}{2} \right) \right)^{\frac{2}{1+B}} \tag{4.17}$$

The model was implemented in 'lazy' way, because the S_p term was considered zero and $S_u = -\tau_w \Delta x \Delta y$. The source term was added only in the first node near to the wall.

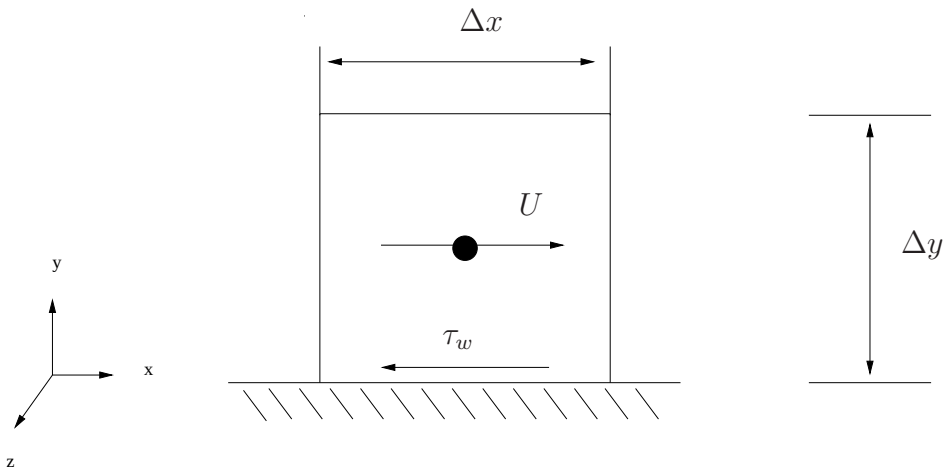

Figure 4.2: Near Wall region

Chapter 5

Results

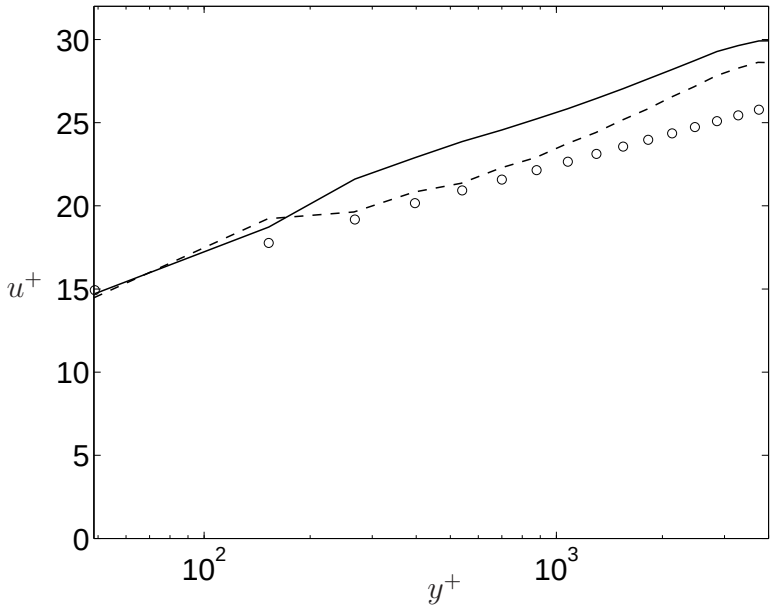

Figure 5.1: Time-averaged velocity profile for Re_τ=4000, $-$ Smagorinsky model, $--$ Wale model, $\circ$ Log-law

The main objective of this report is to implement wall-functions for simulation of channel flow with LES. The Fig.(5.1) illustrates time-averaged velocity profile for $Re_\tau = 4000$ using the Smagorinsky and the Wale model. The Wale model gives better approximation of velocity profile than the Smagorinsky model. The Fig.(5.2) shows the u_{rms}/u^* fluctuations. Near the wall the Wale model gives higher fluctuations than the Smagorinsky model. This is mainly due to the SGS viscosity, see Fig.(5.5), because near the wall we have very high velocity gradient and consequently the SGS viscosity is too high due to the nature of the Smagorinsky model. Higher SGS viscosity will damp velocity fluctuations. As is evident from Fig.(5.3) the $\langle u'v' \rangle / u^{*2}$ quantity determined by the Wale model has some 'wiggles'. One explanation for this could be that the velocity gradients are too high for this mesh. If we look at Fig.(5.4) for the value plotted on faces there is no 'wiggles'. The face value are more relevant because this is what the code is using.

Acording to Eqn.(3.11) $\tau_w = 1$ which is satisfied for averaged value $\langle \tau_w \rangle$ for the Smagorinsky model Fig.(5.6) and also for the Mason-Callen model Fig.(5.7).

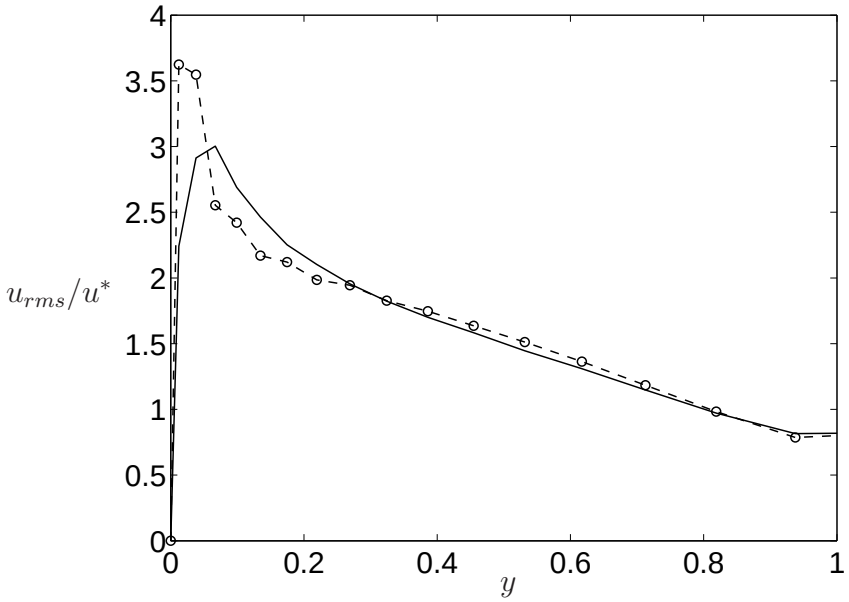

Figure 5.2: – Smagorinsky model, – ∘ – Wale model

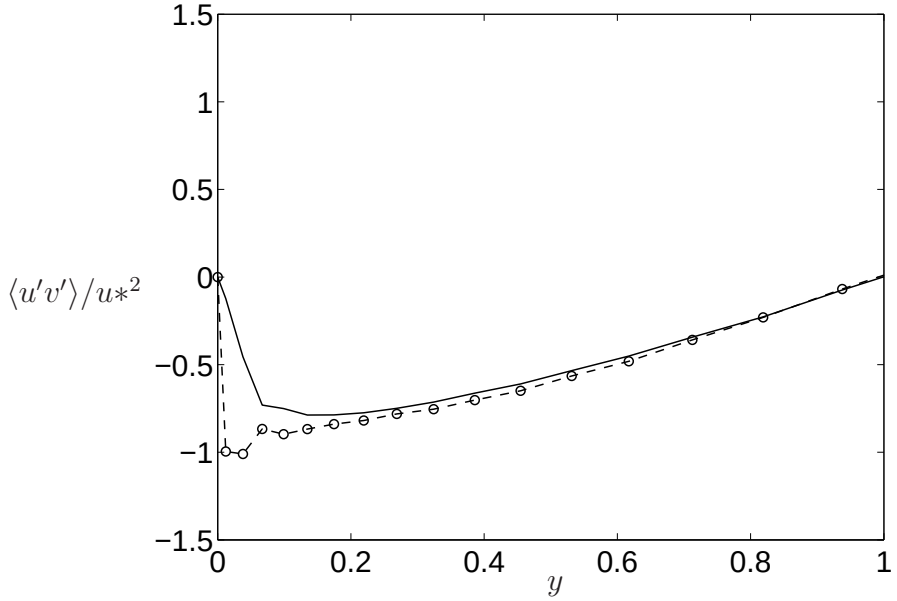

Figure 5.3: – Smagorinsky model, – ∘ – Wale model

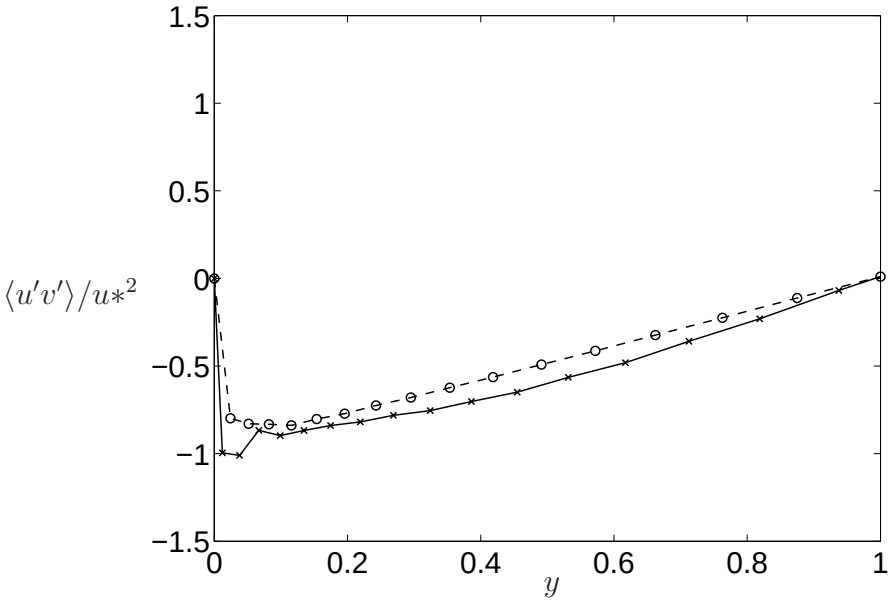

Figure 5.4: $-\times-$ Wale model at p nodes, $-\circ-$ Wale model at faces

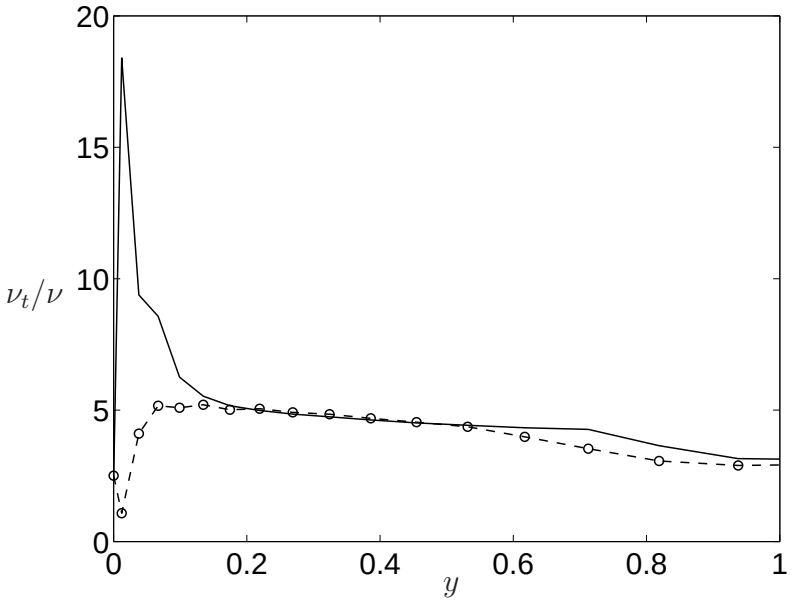

Figure 5.5: $-$ Smagorinsky model, $-\circ-$ Wale model

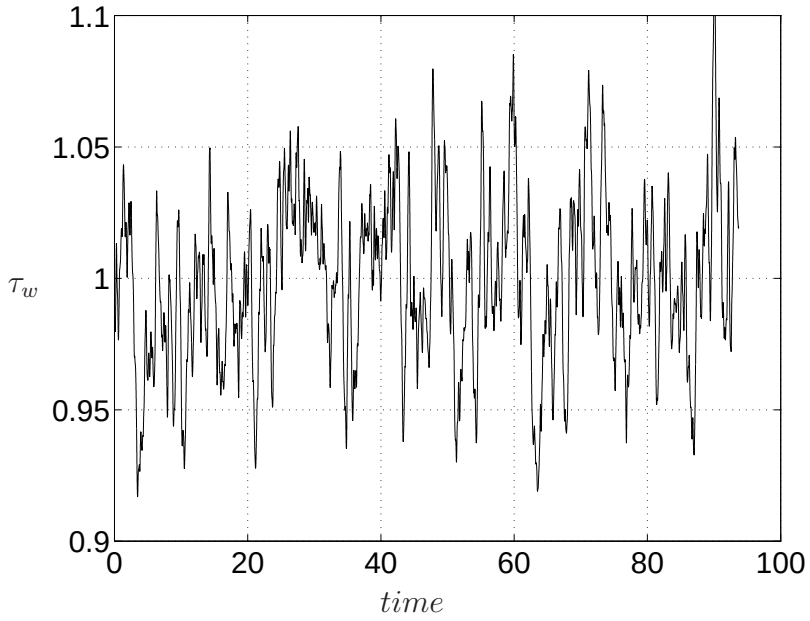

Figure 5.6: Time history for τ_w Smagorinsky model. Mesh A

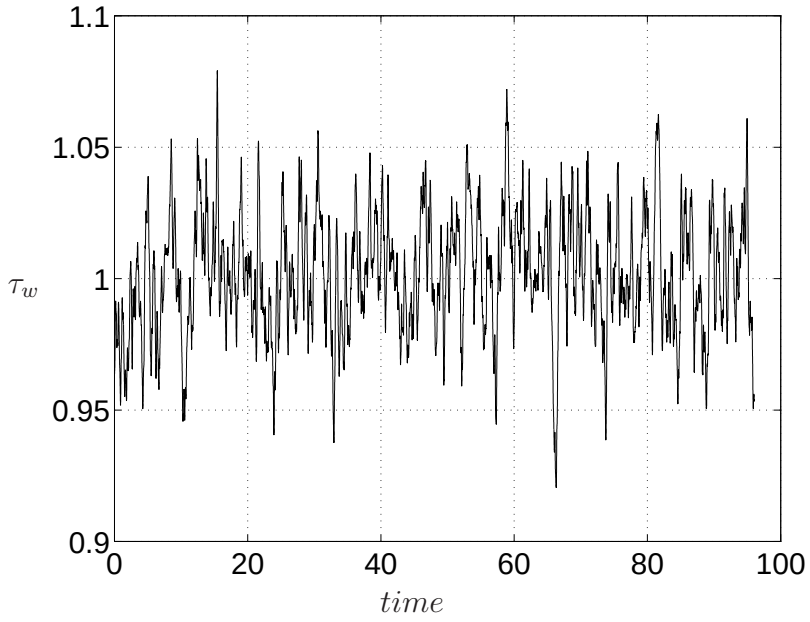

Figure 5.7: Time history for τ_w Mason-Callen model. Mesh A

The derivative $\partial u/\partial y$ near the wall can be calculated in two different modes

1. in a classical way
$$\left(\frac{\partial u}{\partial y}\right)_2 = \frac{u_p(2) - u_p(1)}{y_p(2) - y_p(1)} \tag{5.1}$$

2. using log-law:
$$\left(\frac{\partial u}{\partial y}\right)_2 = \frac{u^*}{\kappa y_p} \tag{5.2}$$

This can be applied only at the first node near the wall. The results presented in Fig.(5.8) for the Smagorinsky model and in Fig.(5.9) for the Wale model show that the viscosity is reduced in the second node and also slightly at the other nodes. Note that the same happens for the fluctuating velocity u_{rms}/u^* see Fig.(5.10).

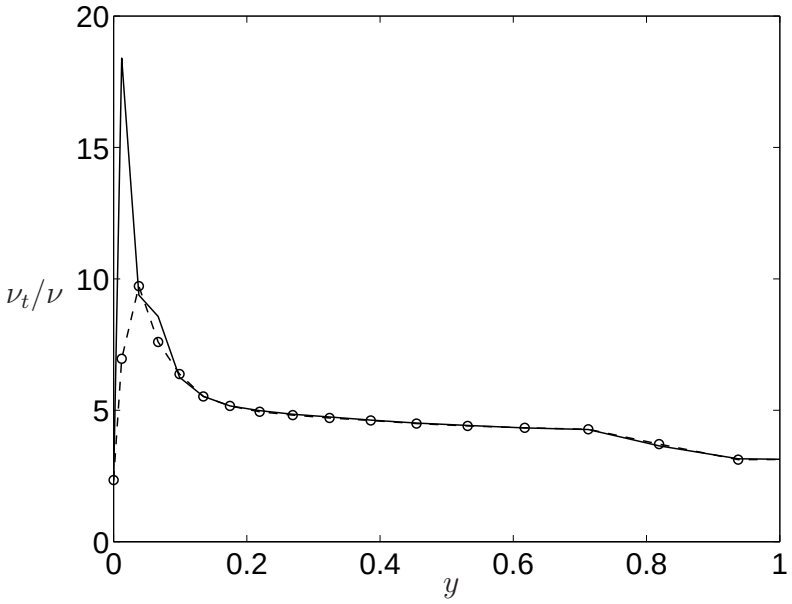

Figure 5.8: Smagorinsky model:– $\left(\frac{\partial u}{\partial y}\right)_2 = \frac{u(2) - u(1)}{y(2) - y(1)}$, $-\circ-$ $\left(\frac{\partial u}{\partial y}\right)_2 = \frac{u^*}{\kappa y_p}$

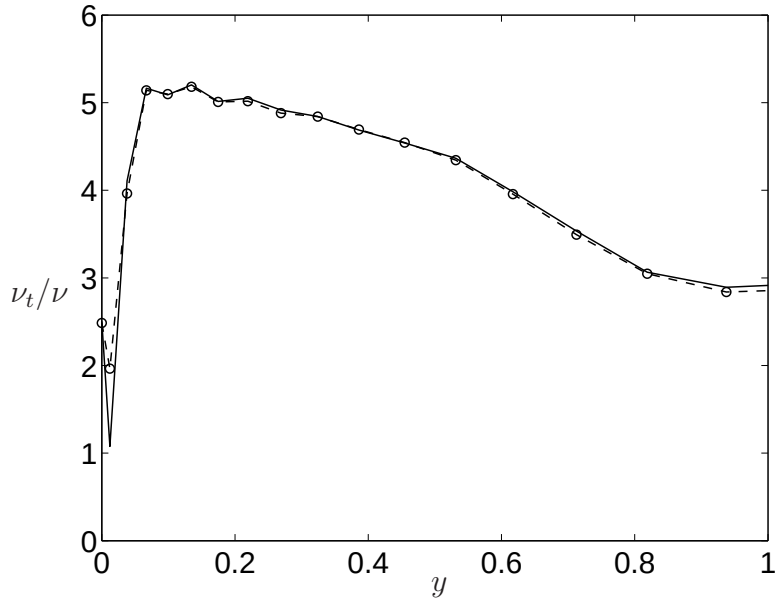

Figure 5.9: Wale model:$-\left(\frac{\partial u}{\partial y}\right)_2 = \frac{u(2)-u(1)}{y(2)-y(1)}, -\circ-\left(\frac{\partial u}{\partial y}\right)_2 = \frac{u^*}{\kappa y_p}$

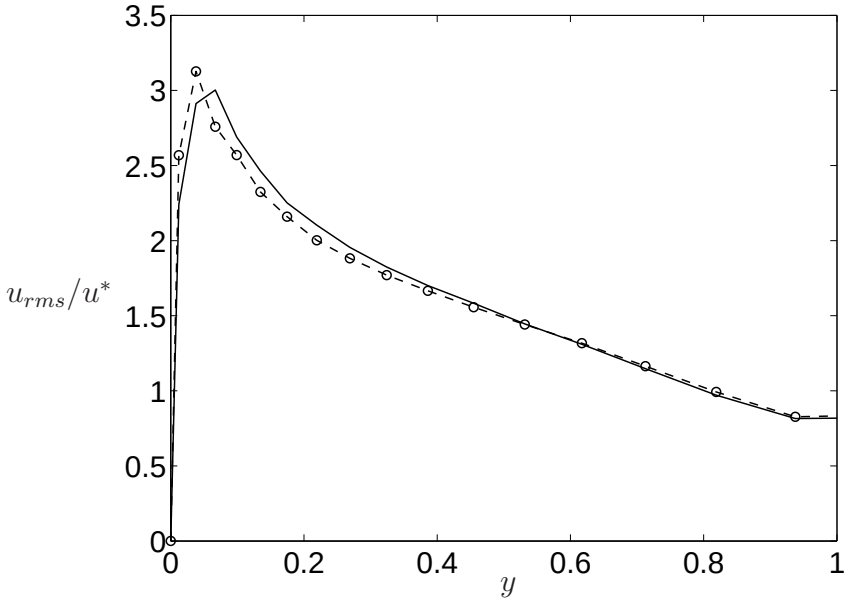

Figure 5.10: Smagorinsky model:$-\left(\frac{\partial u}{\partial y}\right)_2 = \frac{u(2)-u(1)}{y(2)-y(1)}, -\circ-\left(\frac{\partial u}{\partial y}\right)_2 = \frac{u^*}{\kappa y_p}$

	length scale	viscosity at the wall
Smagorinsky/Log-law	Smagorinsky	Log-law
Mason-Callen/Log-law	Mason-Callen	Log-law
Samgorinsky/Werner-Wengler	Smagorinsky	Werner-Wengler

Table 5.1: Length scale model and viscosity model

Next the wall function based on the log-law is used together with the Mason-Callen and the Smagorinsky model. Also the wall function based on power-law using the Werner-Wengler model together with the Smagorinsky model is used. Velocity profile Fig.(5.11) calculated with the Werner-Wengler model gives the best approximation to log-law except near the wall where the velocity is forced to be too low. The Mason-Callen model gives an intermediate profile between the Smagorinsky and the Werner-Wengler model. The value calculated for fluctuating velocity and SGS viscosity Fig.(5.12) and Fig.(5.14) with the Smagorinsky/Log-law and the Smagorinsky/Werner-Wengler model are the same. This mean that the velocity gradients are the same but not velocity profile.

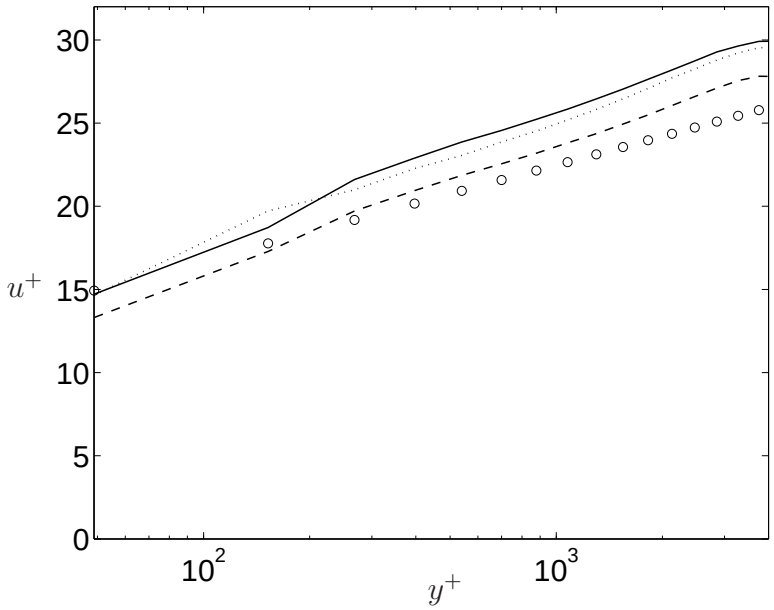

Figure 5.11: Time-averaged velocity profile for Re_τ=4000. $-$ Smagorinsky/Log-law, $\cdots$ Mason-Callen/Log-law, $--$ Smagorinsky/Werner-Wengler

How ν_T is calulated and how the viscosity at the wall is defined, see Table (5.1).

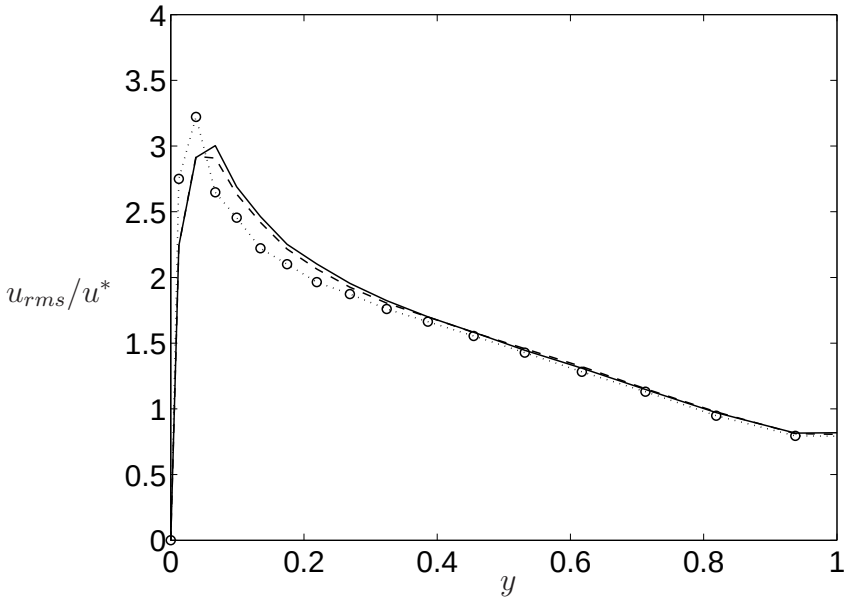

Figure 5.12: – Smagorinsky/Log-law, ··· ○ ··· Mason-Callen/Log-law, −− Smagorinsky/Werner-Wengler

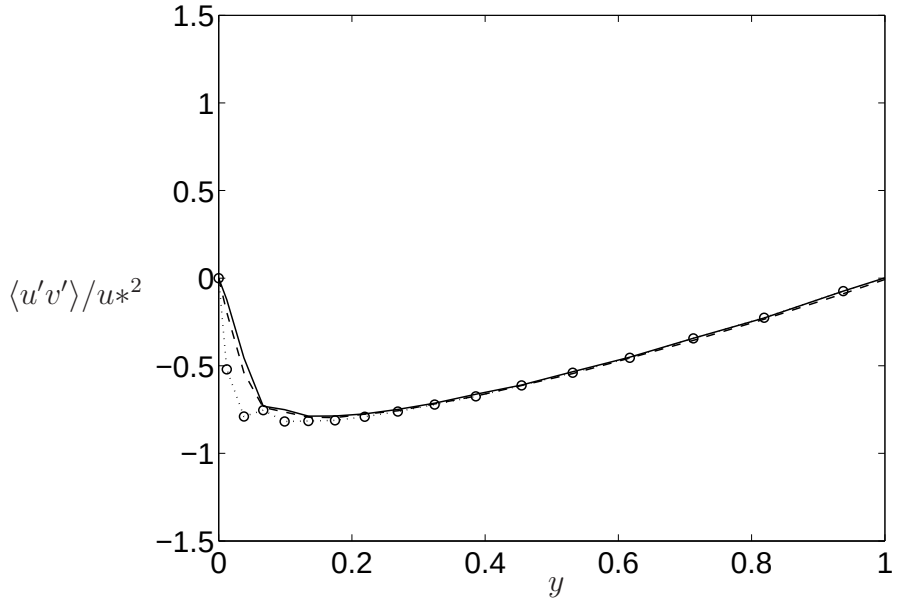

Figure 5.13: −Smagorinsky/Log-law, ··· ○ ···Mason-Callen/Log-law, −−Smagorinsky/Werner-Wengler

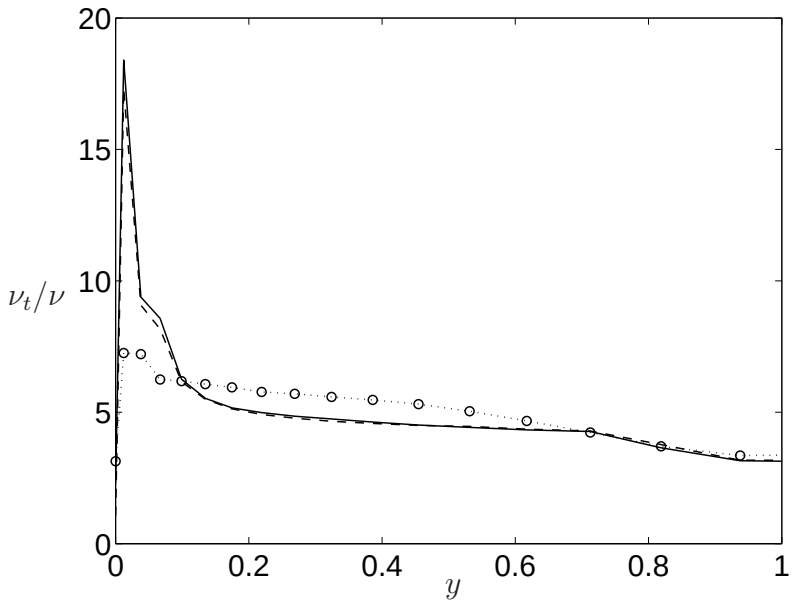

Figure 5.14: – Smagorinsky/Log-law, · · · ◦ · · · Mason-Callen/Log-law, −− Smagorinsky/Werner-Wengler

The main idea with wall-functions is to go as far as possible away from the wall. For $Re_\tau = 16000$ the flow was analyzed using different y^+ 54, 108, 200. The velocity profiles Fig.(5.15) compared with Log-law show almost the same differences for all cases. All three cases are quite close to each other. The same happens for u_{rms}/u^* Fig.(5.16) and the $\langle u'v' \rangle / u^{*2}$ Fig.(5.17); the only problem is near the wall where we have some differences. Not the same can be noticed for the viscosity Fig.(5.18) where for $y^+ = 200$ we have the lowest viscosity. The main reason is that the viscosity is very sensitive to filter width $\overline{\Delta} = (\Delta x \Delta y \Delta z)^{1/3}$ and $\overline{\Delta}_{y^+=200} < \overline{\Delta}_{y^+=108} < \overline{\Delta}_{y^+=54}$.

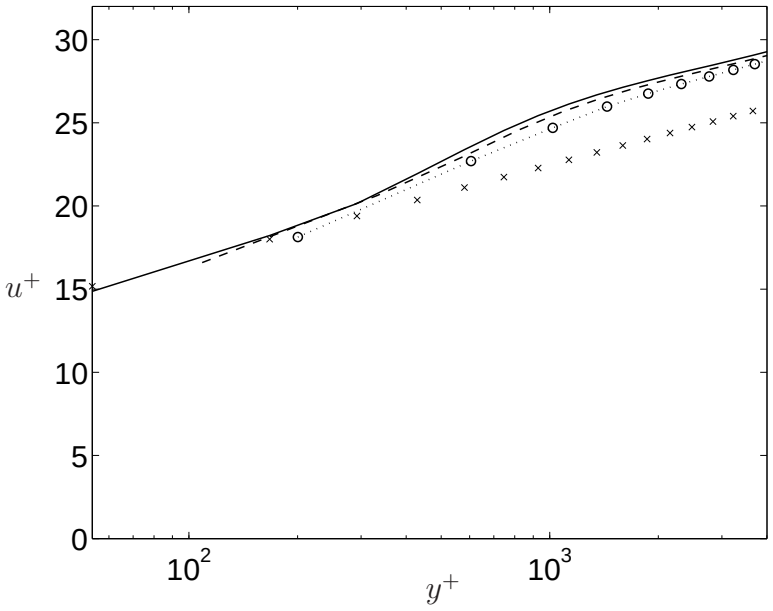

Figure 5.15: Time-averaged velocity profile for Re_τ=16000 using the Smagorinsky model/Log-law with $\left(\frac{\partial u}{\partial y}\right)_2 = \frac{u^*}{\kappa y_p}$ at different y^+; $\times$ Log-law, $-$ $y^+ = 54$, $--$ $y^+ = 108$, $\cdots\circ\cdots$ $y^+ = 200$

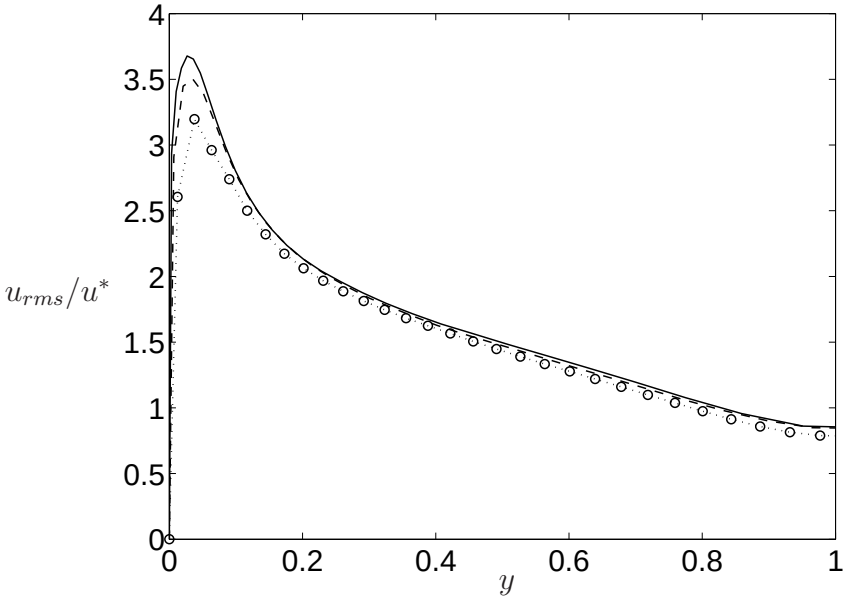

Figure 5.16: $-$ $y^+ = 54$, $- -$ $y^+ = 108$, $\cdots \circ \cdots$ $y^+ = 200$

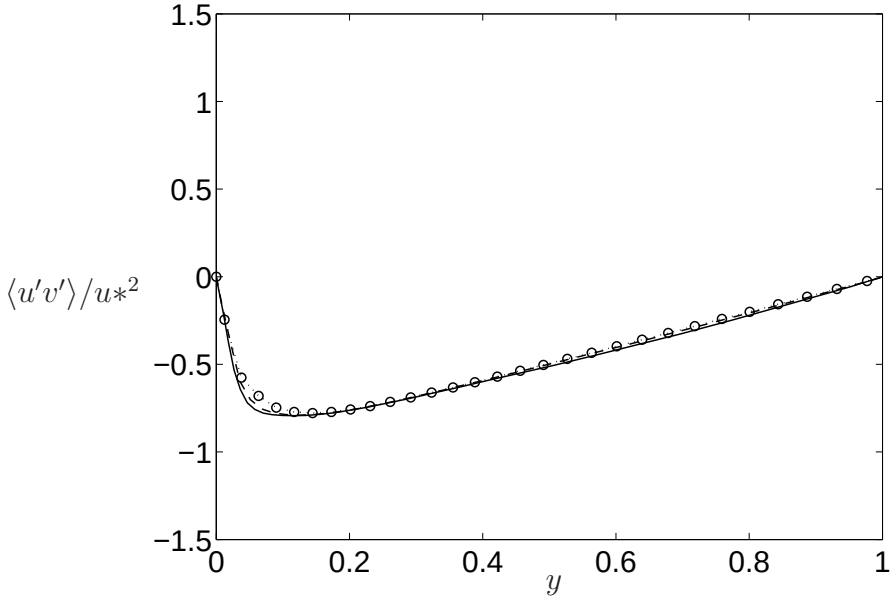

Figure 5.17: $-$ $y^+ = 54$, $- -$ $y^+ = 108$, $\cdots \circ \cdots$ $y^+ = 200$

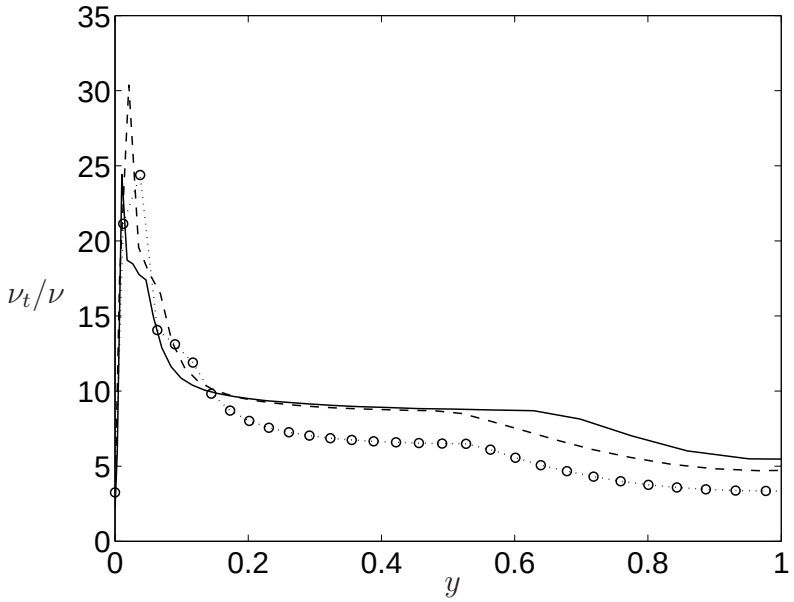

Figure 5.18: $-$ $y^+ = 54$, $- -$ $y^+ = 108$, $\cdots \circ \cdots$ $y^+ = 200$

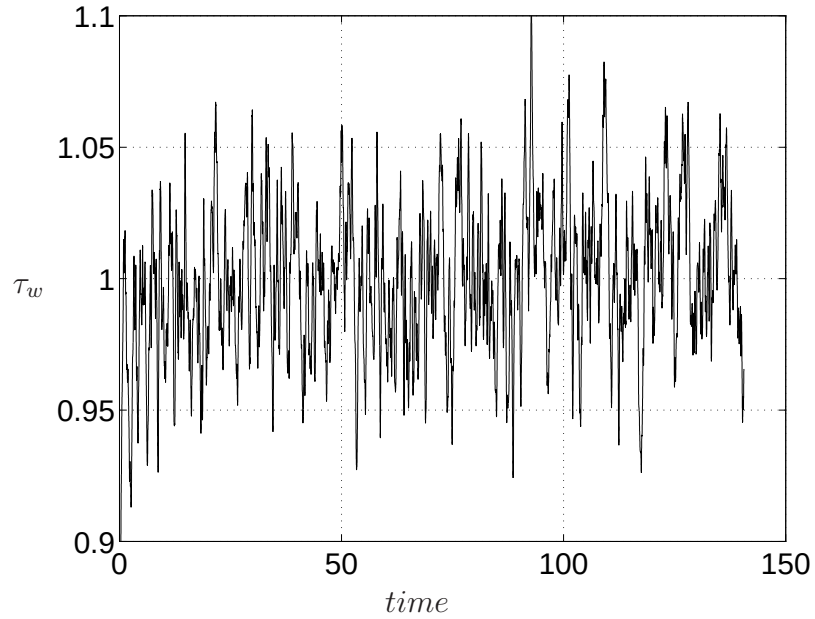

Figure 5.19: Time history for τ_w Smagorinsky model. Mesh C

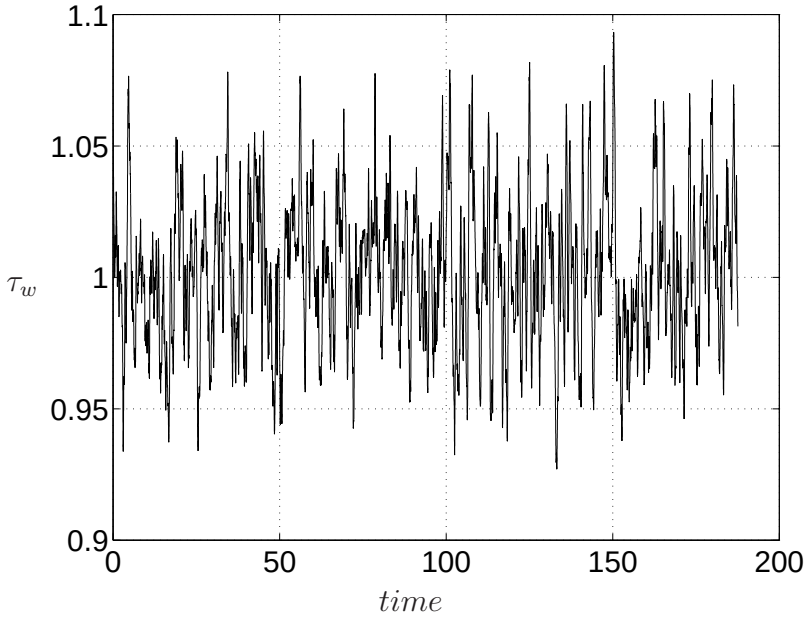

Figure 5.20: Time history for τ_w Smagorinsky model. Mesh D

From Fig.(5.19) and Fig.(5.20) it is clear that $\langle \tau_w \rangle = 1$ which means that the flow is fully developed and there is no acceleration.

Because the comparison for the velocity profile was done all the time with the log-law the question is how should be the mesh in order that the velocity profile to be the same as log-law. In other words how fine the mesh should be? Should the mesh be fine enough in all directions or is it enough to have fine mesh in the direction perpendicular to wall?

As is evident from Fig.(5.21) the best result was obtained when the number of nodes was increased in all three directions. For the finest mesh in Fig.(5.21) the size of length scales are $\Delta x^+ \sim 205$, $\Delta z^+ \sim 103$ and $\Delta y^+_{min} \sim 97$.

The mesh was changed in the following way, first only the y-direction was increased and x, z kept the same, the result was not good; next the y-direction was kept constant and x, z increased the result was better. This mean that it is not enough to have fine mesh normal to the wall it is also important that the mesh in other two directions to be fine enough and respect $\Delta x^+ < 100$, $\Delta z^+ < 50$ to get good results.

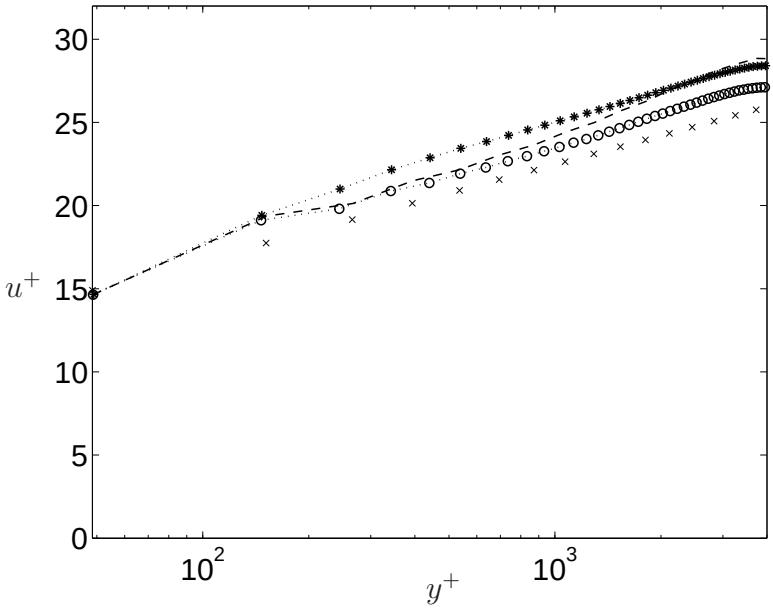

Figure 5.21: $\cdots\star\cdots$ $34 \times 82 \times 34$, $--$ $50 \times 34 \times 60$, $\cdots\circ\cdots$ $50 \times 82 \times 60$, $\times Log - Law$

Conclusions

The Log-law and the Werner-Wengler model have been implemented to define the SGS viscosity at the wall and the Mason-Callen model to calculate the length scale for large eddy simulations. All models give acceptable results comparing with Log-law, when LES are performed using very coarse mesh.

Although the velocity profile is sensitive to model used, this can be improved by increasing Δx^+ and Δz^+. For u_{rms}, v_{rms}, w_{rms}, and uv the propagation into the flow of error introduced by approximate boundary condition are acceptable.

Future Work

First to run a case where we have some experimental or DNS data so to be able to compare not only velocity with log-law but also u_{rms}, v_{rms}, w_{rms}.
Second to see how it works in a case where we have flow around obstacles with sharp edges and corners, or flow with recirculation.

Bibliography

[1] Jonas Bredberg. On the wall boundary condition for turbulence models. Internal report, Dept. of Thermo and Fluid Dynamics, Chalmers University of Technology, Göteborg, Sweden, 2000.

[2] Richard H. Pletcher Dale A. Anderson, John C. Tannehill. *Computational Fluid Mechanics and Heat Transfer*. McGraw-Hill Book Company, 1984.

[3] L. Davidson and S. H. Peng. Hybrid LES-RANS modelling: a one-equation SGS model combined with $k-\omega$ model for predicting recirculating flows. *Int. J. Numer. Meth. Fluids*, 43, 2003.

[4] Lars Davidson and Bijan Farhanieh. CALC-BFC a finite-volume code employing collocated variable arrangement and cartesian velocity componenets for computation of fluid flow and hear transfer in complex three-dimensional geometries. Report 95/11, Dept. of Thermo and Fluid Dynamics, Chalmers University of Technology, Göteborg, Sweden, 1995.

[5] H.Tennekes and J.L.Lumley. *A First Course in Turbulence*. The Massachusetts Institute of Technology, 1972.

[6] H.WERNER and H.WENGLE. Large-eddy simulation of turbulent flow over and around a cube in a plate channel. In Springer-Verlag, editor, *Turbulent Shear Flows 8*, volume 8, Munich, Germany, 1993.

[7] P.J. MASON and N.S.CALLEN. On the macnitude of the subgrid-scale eddy coefficient in large-eddy simulations of turbulent channel flow. *J. Fluid Mechanics*, 162, 1986.

[8] F. Nicoud and F. Ducros. Subgrid-scale stress modelling based on the square of the velocity gradient tensor. *Flow, Turbulence and Combustion*, 62:183–200, 1999.

[9] U.Piomelli. Introduction to the modelling of turbulence. Lectures notes, 2000.

[10] H K VERSTEEG and W MALALASEKERA. *An Introduction to Computational Fluid Dynamics The Finite Volume Method*. Longman Group Ltd, 1995.